JACS
JOURNAL OF THE AMERICAN CHEMICAL SOCIETY
ARTICLE
pubs.acs.org/JACS

Understanding the Preferential Adsorption of CO_2 over N_2 in a Flexible Metal−Organic Framework

Nour Nijem,[†] Peter Thissen,[†] Yanpeng Yao,[‡] Roberto C. Longo,[†] Katy Roodenko,[†] Haohan Wu,[§] Yonggang Zhao,[§] Kyeongjae Cho,[†] Jing Li,[§] David C. Langreth,[‡] and Yves J. Chabal*,[†]

[†]Department of Materials Science and Engineering, University of Texas at Dallas, Richardson, Texas 75080, United States

[‡]Department of Physics and Astronomy and [§]Department of Chemistry and Chemical Biology, Rutgers University, Piscataway, New Jersey 08854, United States

S Supporting Information

ABSTRACT: The unusual uptake behavior and preferential adsorption of CO_2 over N_2 are investigated in a flexible metal−organic framework system, $Zn_2(bdc)_2(bpee)$, where bpdc = 4,4′-biphenyl dicarboxylate and bpee = 1,2-bis(4-pyridyl)ethylene, using Raman and IR spectroscopy. The results indicate that the interaction of CO_2 with the framework induces a twisting of one of its ligands, which is possible because of the type of connectivity of the carboxylate end group of the ligand to the metal center and the specific interaction of CO_2 with the framework. The flexibility of the bpee pillars allows the structure to respond to the twisting, fostering the adsorption of more CO_2. DFT calculations support the qualitative picture derived from the experimental analysis. The adsorption sites at higher loading have been identified using a modified van der Waals− Density Functional Theory method, showing that the more energetically favorable positions for the CO_2 molecules are closer to the C═C bond of the bpee and the C−C bond of the bpdc ligands instead of the benzene and pyridine rings of these ligands. These findings are consistent with changes observed using Raman spectroscopy, which is useful for detecting both specific guest−host interactions and structural changes in the framework.

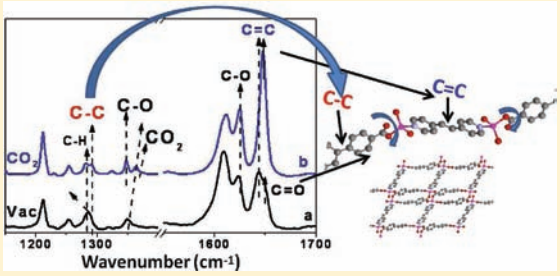

1. INTRODUCTION

Metal−organic frameworks (MOFs) have attracted much attention in a variety of fields such as gas separation and storage, catalysis and sensing, and polymers.[1−6] Compared to activated carbon and zeolites, MOFs have much higher surface areas (the largest reported is for MIL-101, with a Langmuir surface area of 5900 m^2/g),[7] and their structures can be easily tailored. Different pore size/shape and functionalities can be achieved by simply selecting the metal center and/or the ligand. A unique property of some of these frameworks is their flexibility, allowing reversible structural changes to occur as a response to external stimuli such as guest inclusion.[8−17] Such changes have been identified by the appearance of a step (gate opening) and a hysteresis in the adsorption/desorption measurements.[18−20] An in-depth understanding of the mechanisms involved cannot be derived using solely these physical measurements. Therefore, X-ray diffraction (XRD) techniques have been utilized to understand this gate-opening mechanism.[21,22] Although XRD data have proven valuable for the characterization of geometrical transformation of MOFs,[23−25] this technique is not sensitive to changes that do not cause geometrical transformation and systems with no long-range periodicity. Moreover, in situ XRD is not readily available, and the analysis of the data is challenging.

Vibrational spectroscopy such as infrared (IR) or Raman spectroscopy, on the other hand, is common and offers relatively simple data analyses. Consequently, vibrational techniques have been implemented to study the interactions of guest molecules in MOFs and to characterize MOF films.[18,26−35] However, investigation of the breathing effects in *flexible* MOFs using IR and Raman spectroscopy has been limited to a few samples, such as MIL-53(Ga,Cr).[18] More work needs to be done to understand the factors that will make it possible to choose the ligands for optimum flexibility and desired selective adsorption.

In this work, a novel, flexible, microporous MOF was selected to investigate the mechanisms involved in gate-opening phenomena, $Zn_2(bpdc)_2bpee$, where bpdc = 4,4′-biphenyl dicarboxylate and bpee = 1,2-bis(4-pyridyl)ethylene. This MOF is composed of two types of ligands arranged in a three-dimensional interpenetrated structure with one-dimensional parallelogram-shaped micropore channels running along the *b*-axis (window size ∼5 × 7 Å; see Figure S1 in the Supporting Information). Each Zn metal center is tetrahedrally coordinated to three carboxylate groups from three bpdc ligands. The two ends of the bpdc ligand bond to the metal center in two different ways, one bidentate and the other monodentate. Two bidentate carboxylate groups from two centrosymetrically related bpdc ligands are coordinated to two different Zn centers to form the eight-membered ring $Zn_2(COO)_2^{2+}$ secondary building unit (SBU). The bpdc ligands form 2D interpenetrated nets, and

Received: June 2, 2011
Published: July 07, 2011

the metal center is further connected to the bpee pillars to form the 3D framework.[36,37] $Zn_2(bpdc)_2bpee$ crystallizes in the monoclinic crystal system (space group $C2/c$) with a solvent-accessible volume of 1171.9 $Å^3$ and a Langmuir surface area of 483 m^2/g .

$Zn_2(bpdc)_2bpee$ exhibits a preferential adsorption of CO_2 over several other gases, characterized by a step (at ~0.1 atm) in the adsorption/desorption curve.[36,37] At this inflection point (~0.1 atm), changes in the binding energies are observed. On the other hand, N_2 does not adsorb under similar conditions, even at pressures higher than the inflection point for CO_2. To explain these properties, the origin of the affinity for CO_2 over other gases and the reason for the structure's remarkable flexibility need to be determined.

This study addresses these fundamental questions by utilizing IR and Raman spectroscopy techniques in conjunction with Density Functional Theory (DFT) calculations. IR and Raman spectroscopy are complementary techniques, with different selection rules, and have recently been implemented to study adsorption of gases into MOFs.[27,29−31] Using these spectroscopic techniques, we have monitored changes occurring on specific bonds in the MOF structure, which can be correlated to MOF structural changes and guest−host interactions.

2. MATERIALS AND METHODS

2.1. Materials Synthesis[36]. *Synthesis.* Pure phases of $Zn_2(bpdc)_2(bpee)\cdot 2DMF$ polycrystalline samples were solvothermally synthesized by mixing $Zn(NO_3)_2\cdot 6H_2O$ (0.0892 g, 0.30 mmol), 4,4-biphenyldicarboxylic acid (H_2bpdc, 0.0727 g, 0.30 mmol), and 1,2-bipyridylethene (bpee, 0.0547 g, 0.30 mmol) in a molar ratio of 1:1:1 in 15 mL of dimethylformamide (DMF) solution. The reaction container was slowly heated to and kept at 170 °C for 3 days and then cooled to room temperature at a rate of 0.1 °C/min. Light yellow powders (0.0726 g, 52% yield) of the title compound were obtained by filtering, washing with DMF three times, and drying in a vacuum oven.

Sample Activation. Activation of the sample was carried out through solvent exchange with chloroform for 3 days and then dichloromethane for 4 days. The sample was then dried in a vacuum at room temperature.

2.2. IR and Raman Spectroscopy. IR absorption spectroscopy measurements of CO_2 adsorption were performed in transmission mode at room temperature using a liquid-N_2-cooled indium antimonite detector. Approximately 10 mg of the activated MOF was lightly pressed onto a KBr support, mounted in a high-temperature, high-pressure cell (Specac product no. P/NH 5850c), and heated to 120 °C in a vacuum (100 mTorr) for complete desolvation. Subtraction of the CO_2 gas phase under these conditions is necessary and is described in detail in section 2 of the Supporting Information.

Raman spectroscopy measurements were performed using a solid-state 532 nm laser. The activated sample was loaded into a Linkam FTIR600 cooling/heating stage, and the sample was heated to 120 °C in a vacuum (900 mTorr) for dehydration. A laser power of 1−10% (0.113−1.23 mW) was used to avoid degradation of the sample under the laser beam during the Raman measurements.

2.3. Theoretical Methods. To illustrate the effects of possible structural distortions of the MOF ligands, i.e., changes in the C−C inter-ring bond length or twisting angles, on the Raman frequencies, we perform first-principle simulations. The calculations were performed using DFT within the generalized gradient approximation (GGA) as implemented in the Vienna ab initio simulation package (VASP).[38] The electron−ion interaction is described by the projected−augmented wave (PAW) scheme. The electronic wave functions are expanded into plane waves up to a kinetic energy of 400 eV. The system is modeled by periodically repeated supercells. Each supercell consists of 156 atoms. All atoms are allowed to relax until the forces on them are below 20 meV/Å. Brillouin zone integration is performed using 3×3×3 Monkhorst−Pack meshes. We use the PW91 functional to describe the electron exchange and correlation energy within the GGA.

On the other hand, the adsorption of CO_2 and N_2 molecules within $Zn_2(bpdc)_2(bpee)$ structure is dominated by van der Waals (vdW) interactions, which cannot be correctly described by GGA. To capture this interaction, we apply calculations using the modified van der Waals−density Functional Theory method (vdW-DFT2) developed by our group and collaborators[39−42] and implemented in ABINIT.[43,44] Previously, vdW-DFT2 has been successfully applied to calculate the binding energies, vibrational modes, etc., for various sparse systems.[39−42,45−49] We use Troulier−Martin types of pseudopotentials[50] for the nuclear and core electrons and a plane wave basis set to expand the valence electron wave functions. The Zn 3d electrons are considered as valence electrons. To ensure a proper convergence, a cutoff energy of 680 eV is used for the plane wave basis. We start from the experimental structure and atomic positions with open pores and relax both the unit cell parameters and the atomic positions of the $Zn_2(bpdc)_2(bpee)$ with Perdew−Burke−Ernzerhof (PBE) GGA exchange-correlation.[51] We then fix the atomic positions of $Zn_2(bpdc)_2(bpee)$ and relax the CO_2's within the MOF structure using vdW-DFT2. The Hellman−Feynman forces on the CO_2 atoms are converged to within 0.05 eV/A. Vibration modes of the adsorbed CO_2 molecules are calculated using the frozen phonon method. Our calculation yields a binding energy of 33.7 kJ/mol, which reproduces the experimental value of 32.5−33.5 kJ/mol very well.[37]

3. RESULTS

3.1. Spectroscopic Characterization of CO_2 Interaction and Structural Changes in $Zn_2(bpdc)_2(bpee)$. *IR and Raman Characterization of CO_2 Interactions below and above the Transition Point (P_{open} = 0.1 atm).* To understand the interaction of CO_2 with $Zn_2(bpdc)_2(bpee)$ below the inflection point (<0.1 atm), we performed IR measurements of CO_2 adsorption at room temperature and low pressures (2.6×10^{-3}−7.8×10^{-3} atm, 2−6 Torr). Figure 1 presents the IR absorption spectra of (top) activated $Zn_2(bpdc)_2(bpee)$ in a vacuum, referenced to KBr in a vacuum, and (bottom) CO_2 adsorbed in $Zn_2(bpdc)_2(bpee)$ after subtraction of the contributions from gas-phase CO_2 (see Supporting Information section 2). An IR band at 2334 cm^{-1} is observed, indicating a ~−15 cm^{-1} red-shift (from the unperturbed value at 2349 cm^{-1}) of the asymmetric C═O stretch mode of the CO_2. The shoulder at 2322 cm^{-1} is a combination of the stretching band and the two bending modes of adsorbed CO_2 ($\nu_3-(\delta_1-\delta_2)$). The IR measurements can be performed only below the transition point (0.1 atm) because the CO_2 gas phase has a very strong absorption at higher CO_2 pressures and the gas phase cannot be readily subtracted. Raman spectra are collected for the guest-free MOF in a vacuum and after introduction of 1 bar of CO_2 at room temperature. Figure 2 presents the Raman spectra of activated $Zn_2(bpdc)_2(bpee)$ in a vacuum (~900 mTorr) and under atmospheric pressure of CO_2. The band corresponding to the adsorbed CO_2 is identified at ~1377 cm^{-1} and is attributed to the symmetric C═O stretch mode. It is ~−11 cm^{-1} red-shifted from the unperturbed value at 1388 cm^{-1}.

Structural Changes with the Adsorption of CO_2 at Room Temperature Identified by Raman Spectroscopy. To identify and interpret the structural changes occurring in $Zn_2(bpdc)_2(bpee)$ upon adsorption of CO_2, it is necessary to assign the MOF Raman bands observed in a vacuum to the specific bonds in

the structure, using previously published assignments.[52,53] We performed Raman spectroscopy measurements at room temperature, comparing samples in a vacuum and in CO_2 at atmospheric pressure, as shown in Figure 2. The right panel of Figure 2 presents an expanded view of the 1200−1500 cm^{-1} region for clarity. The band at 1377 cm^{-1}, corresponding to CO_2 adsorbed in the MOF, is weaker and broader at room temperature than the modes due to the MOF itself. The CO_2 signal becomes clearer at lower temperatures. Some prominent changes in the bands corresponding to the MOF itself are apparent after the introduction of CO_2. Focusing on the high-frequency region (1500−1800 cm^{-1}) first, it is apparent that the intensity of the shoulder at 1650 cm^{-1}, corresponding to the uncoordinated C═O stretch of the bpdc ligand, has decreased. A ∼+4 cm^{-1} blue-shift of the band at 1644 cm^{-1}, corresponding to the C═C stretch in the ethylene of the bpee ligand, is also observed. The broad modes at 1610 and 1625 cm^{-1} are identified as the in-plane pyridyl ring stretch and the asymmetric stretch of the bidentate C−O of the bpdc ligand connected to the Zn metal center, respectively. The corresponding symmetric stretch of the coordinated C−O is at 1430 cm^{-1} (not shown). A ∼+10 cm^{-1} blue-shift of the band at 1355 cm^{-1}, corresponding to the coordinated C−O symmetric stretch, and a ∼−3 cm^{-1} red-shift of the band at 1286 cm^{-1}, corresponding to the C−C inter-ring stretch in the bpdc ligand, are also observed. These observations point to structural changes of the MOF with the adsorption of CO_2. Only the bands at 1293 and 1348 cm^{-1} show no change and are assigned to the C−H stretch and the in-plane deformation mode of the pyridyl ligand, respectively. In contrast to CO_2, no changes are observed upon adsorption of N_2 at room temperature and 1 atm pressure, as shown in Figure S3 in the Supporting Information.

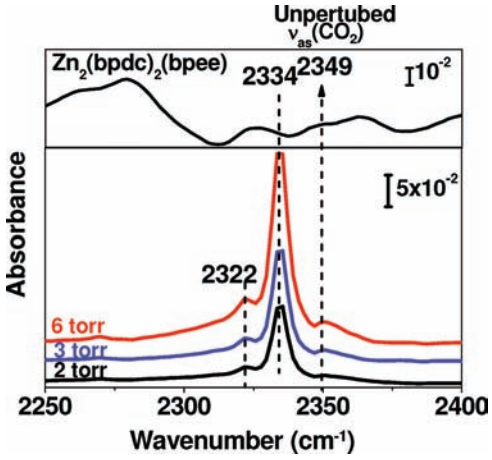

Figure 1. IR absorption spectra of (top) activated $Zn_2(bpdc)_2(bpee)$ in a vacuum and (bottom) adsorbed CO_2 at room temperature and pressures (2−6 Torr). A ∼−15 cm^{-1} red-shift of the asymmetric stretch of CO_2 is observed. Gas phase subtracted.

3.2. Higher Loading of CO_2 and N_2 Adsorption in $Zn_2(bpdc)_2(bpee)$. Lowering the temperature is a convenient way to increase gas loading in MOFs. To distinguish temperature effects from gas-loading effects, we first measured the Raman spectrum of the MOF in a vacuum as a function of temperature and then investigated the changes occurring upon CO_2 and N_2 incorporation.

Low-Temperature Dependence of the MOF Raman Bands in a Vacuum. Figure 3 summarizes the Raman spectra of $Zn_2(bpdc)_2(bpee)$ in a vacuum in the temperature range 25 to −190 °C: the left panel shows the frequency range 1200−1700 cm^{-1}, and the right panel shows the range 1300−1400 cm^{-1}. An increase in the integrated area of the bands at 1654 and 1356 cm^{-1}, corresponding to the uncoordinated C═O stretch and the Zn-coordinated C−O stretch of the bpdc ligand, is observed. The integrated area of the band at 1654 cm^{-1}, corresponding to ν(C═O), increases by 6-fold as the temperature is reduced to −190 °C. This increase in Raman intensity suggests that a change in the relative position of the C═O bond around the carbon takes place, affecting the Raman intensity of both the C−O and the C═O bands. Moreover, a decrease in intensity of the band at 1286 cm^{-1}, corresponding to C−C inter-ring stretch, is observed.

Temperature Dependence of the MOF Raman Bands in the Presence of CO_2. Raman spectra were then recorded as a function of temperature in the presence of atmospheric pressure of CO_2 (pressure maintained down to −60 °C), and they are summarized in Figure 4: the left panel shows the Raman spectra as a function of temperature in the frequency range 1200−1700 cm^{-1}, and the right panel provides an expanded view of the 1300−1400 cm^{-1} region. The band at 1363 cm^{-1}, attributed to the monodentate C−O stretch mode, sharpens as the temperature is lowered. The band at 1377 cm^{-1}, attributed to the symmetric stretch of the C═O mode of CO_2, also sharpens with decreasing temperature. In addition, the band at 1646 cm^{-1},

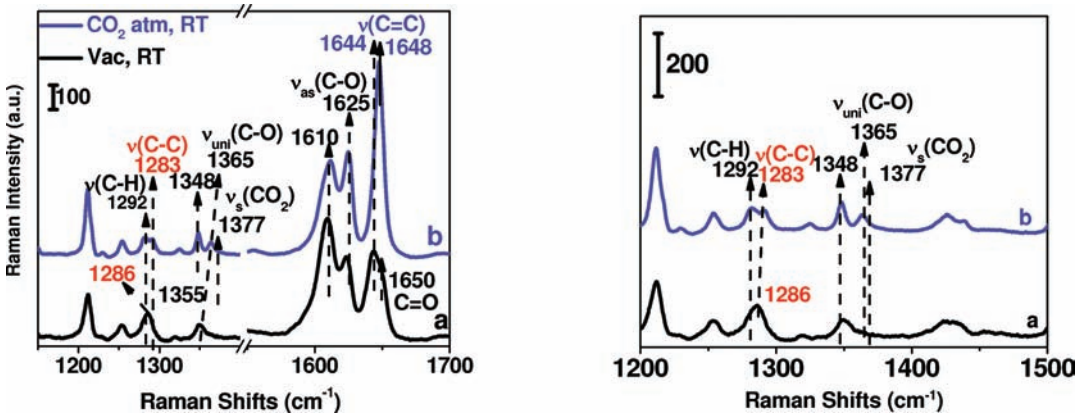

Figure 2. (Left) Raman spectra of activated $Zn_2(bpdc)_2(bpee)$ in a vacuum (a) and after introduction of 1 atm of CO_2 at room temperature (b). (Right) A zoom-in of the 1200−1500 cm^{-1} region.

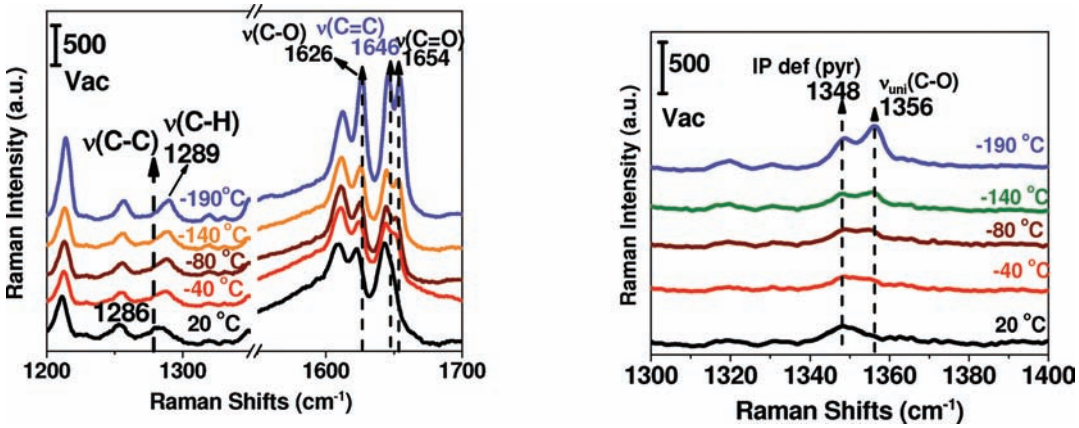

Figure 3. Raman spectra of $Zn_2(bpdc)_2(bpee)$ as a function of temperature in a vacuum, showing two different regions of the spectra.

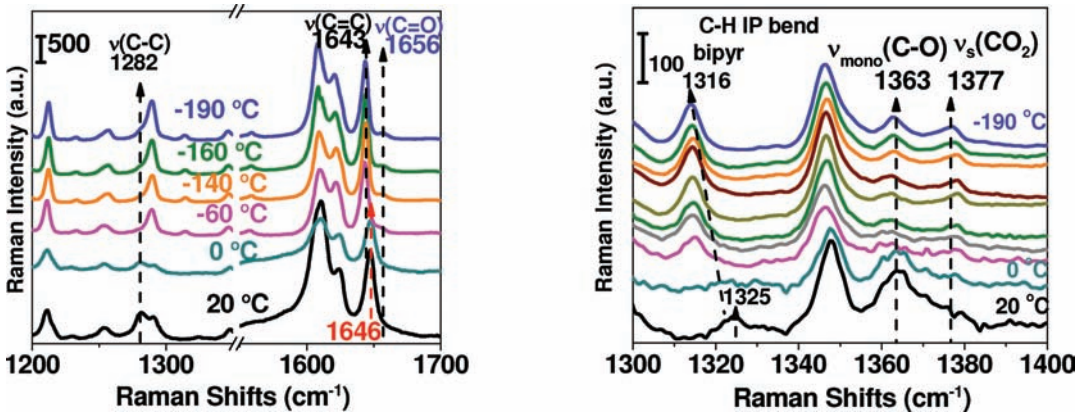

Figure 4. (Left) Raman spectra of CO_2 as a function of temperature and (right) a zoom-in of the 1300−1400 cm^{-1} region.

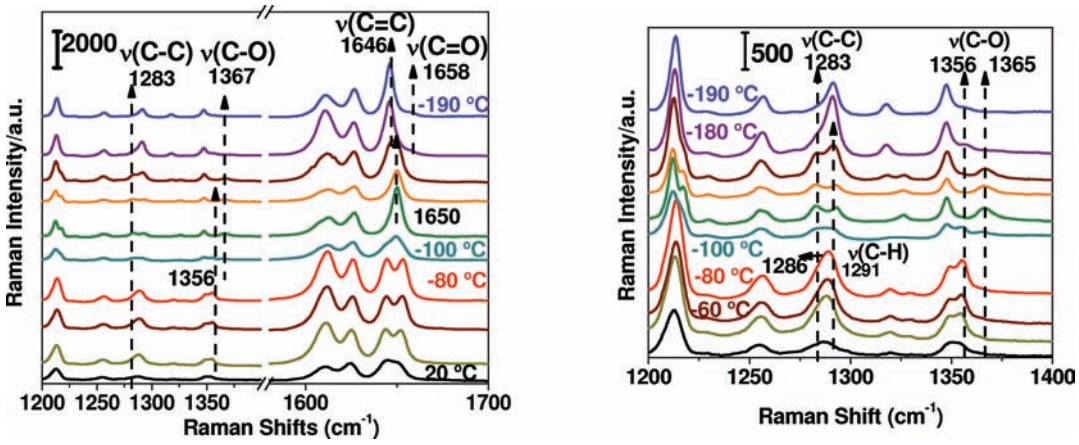

Figure 5. (Left) Raman spectra of $Zn(bpdc)_2(bpee)_2$ N_2 adsorption as a function of temperature. Atmospheric pressure of N_2 is introduced at room temperature. (Right) A zoom-in of the 1200−1400 cm^{-1} region.

corresponding to the C═C stretch of the bpee ligand, red-shifts by ∼−3 cm^{-1}, and the band at 1283 cm^{-1}, corresponding to the C−C inter-ring stretch of the bpdc ligand, weakens.

Temperature Dependence of N_2 Adsorption. Since N_2 does not adsorb at room temperature, we have investigated its behavior as a function of temperature by recording Raman spectra upon cooling in the presence of atmospheric pressure of N_2. Figure 5 shows the Raman spectra in the temperature range 20 to −190 °C: the left panel shows the spectra in the frequency range 1200−1700 cm^{-1}, and the right panel shows an expanded view of the 1200−1400 cm^{-1} region. The changes observed are similar to what happens upon cooling in a vacuum to −80 °C; thereafter, the behavior changes when N_2 is incorporated into the MOF. The band at 1658 cm^{-1}, corresponding

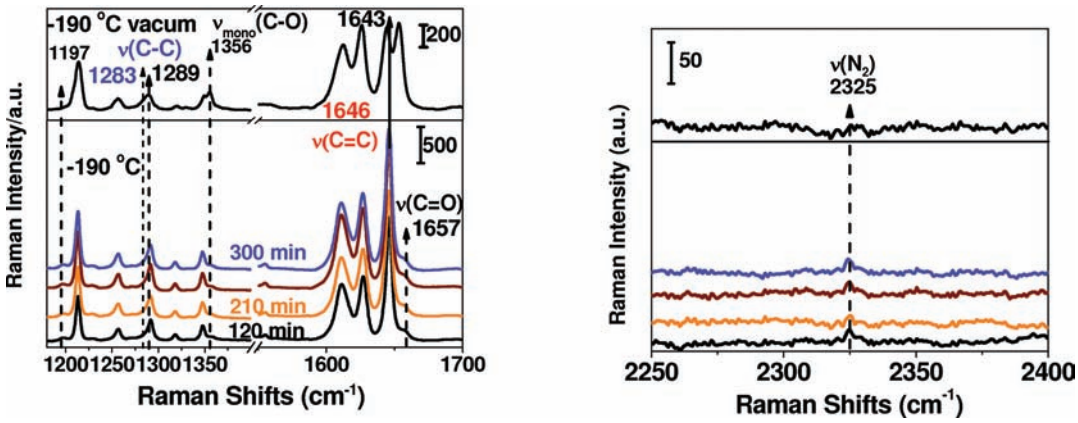

Figure 6. (Left) Raman spectra of N_2 adsorption at −190 °C as a function of time. (Right) A Raman band of adsorbed N_2.

Table 1. Summary of the Changes of the Raman Bands as a Function of Adsorption Gas and Temperature

	ν_{vac} (cm^{-1})		$\Delta\nu$ (cm^{-1})			
Raman bands	room temp	−190 °C	CO_2, room temp	CO_2, −190 °C	N_2, −120 °C	N_2, −190 °C
C═O (bpdc)	1650	+4	NA	NA	NA	+7
C−O−Zn (bpdc)	1355	NA	∼+10	NA	+10	NA
C−C (bpdc)	1286	NA	∼−3	∼−4	−3	−3
C═C (bpee)	1644	+2	+4	−1	+6	+2

to the C═O stretch, weakens, and the band at 1644 cm^{-1}, corresponding to the C═C in the bpee ligand, blue-shifts by ∼+6 cm^{-1}. There is also a ∼+9 cm^{-1} blue-shift of the band at 1356 cm^{-1}, corresponding to the stretch of the coordinated C−O bond in the monodentate carboxylate, and a ∼−3 cm^{-1} red-shift of the band at 1286 cm^{-1}, corresponding to the C−C inter-ring stretch of the bpdc ligand. Cooling below −180 °C results in spectra similar to those obtained upon introducing N_2 directly at −190 °C. These include a ∼−4 cm^{-1} red-shift of the band at 1650 cm^{-1}, accompanied by a red-shift of the band at 1365 cm^{-1}, corresponding to the stretch modes of the monodentate coordinated C−O bond in the bpdc ligand. A decrease in intensity of the band at 1283 cm^{-1} of the C−C bond is also observed.

3.3. Spectroscopic Characterization of N_2 Adsorption at −190 °C. *Adsorption of N_2 at −190 °C.* Isotherm measurements performed at −196 °C (77 K) show a peculiar shape and a step.[37] To understand the changes occurring due to N_2 adsorption, we performed Raman spectroscopy, introducing N_2 when the MOF was at −190 °C. Figure 6 shows the Raman spectra of $Zn_2(bpdc)_2(bpee)$ in a vacuum at −190 °C (left top) and after introduction of N_2 at −190 °C (left bottom) as a function of time. There is a blue-shift (∼+7 cm^{-1}) and a large decrease in intensity of the C═O band at 1650 cm^{-1} and a decrease in intensity of the band at 1356 cm^{-1}, attributed to the monodentate connected C−O stretch of the bpdc ligand. The right panel of Figure 6 shows a weak band at 2325 cm^{-1}, attributed to adsorbed N_2 (red-shifted by ∼−5 cm^{-1} from the unperturbed value to 2330 cm^{-1}). The adsorption of N_2 is also confirmed by high-pressure IR measurements of adsorbed N_2, shown in Figure S4 in the Supporting Information.

The position of the Raman bands for the guest-free MOF at room temperature and their shifts as a function of temperature in a vacuum and in the presence of a guest are summarized in Table 1.

4. DISCUSSION

To understand how Raman and IR absorption spectroscopy can be used to characterize structural changes, it is helpful to summarize the physical mechanisms involved in each technique. IR absorption is sensitive to the dynamic dipole moment of species and is a probe of the transition from the ground to the first excited vibrational state.[53] In contrast, Raman scattering involves excitation from the ground state to a virtual electronic state and an inelastic decay to a level that is typically one vibrational quantum away from the ground state. Raman spectra therefore represent shifts from the incident visible excitation wavelength.[53] Furthermore, Raman is sensitive to the dynamic changes in polarizability. In contrast to IR absorption, which is sensitive to the dynamic dipole moment, Raman activity is based on a change in polarizability, $\partial\alpha/\partial q \neq 0$, where α is the polarizability and q is the nuclear displacement, during vibrational excitation.[53] Therefore, the nonsilent normal modes of centrosymetric molecules with a center of inversion are either Raman or IR active. For example, the C═O asymmetric stretch (2349 cm^{-1}) in CO_2 is only IR active, and the symmetric stretch of the C═O (1388 cm^{-1}) is only Raman active, hence the necessity to combine both techniques.

4.1. Structural Changes Caused by CO_2 Adsorption in $Zn_2(bpdc)_2(bpee)$. Changes observed in the Raman bands of the $Zn_2(bpdc)_2(bpee)$ in the presence of CO_2 indicate that CO_2 induces structural changes in the MOF itself. $Zn_2(bpdc)_2(bpee)$ have shown a preferential adsorption for CO_2 over N_2 at room temperature.[37] The isotherms of CO_2 plotted on a logarithmic scale as a function of pressure (Figure S5 in the Supporting Information) show a rise in CO_2 uptake above 0.1 atm, reaching a

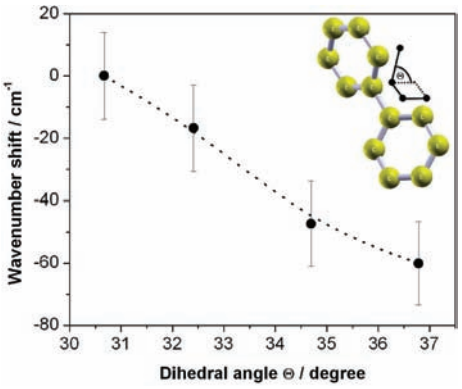

Figure 7. Calculated frequency shifts of the C−C band as a function of the angle change between the two rings in the bpdc ligand.

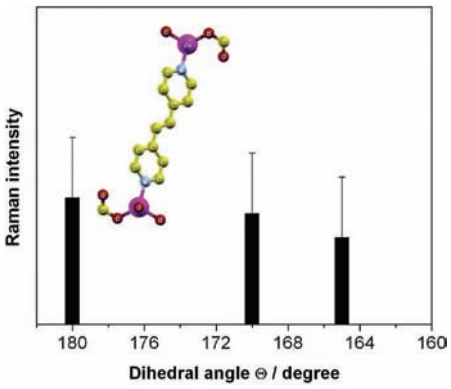

Figure 8. Calculated Raman intensity of the free C═O as a function of dihedral angle between the two C═O on top and bottom of the bpee ligand shown in the inset.

value corresponding to ∼1 CO_2 molecule/unit cell at a pressure of 0.13 atm.

Twisting of the Two Benzene Rings in the bpdc Ligand. The ∼−3 cm^{-1} red-shift of the band centered at 1286 cm^{-1}, associated with the C−C inter-ring of the bpdc ligand, suggests that there is a softening of that bond caused by the presence of the CO_2. If this bond softens, a twist of the two benzene rings in the bpdc ligand is then expected because, under constraint, these two benzene rings are not bonded with the same rigidity. Indeed, there is a monodentate connection of the carboxylate unit at one end of the bpdc ligand (leaving one C═O uncoordinated at that node), while the other end has a rigid bidentate bonding configuration. To test the hypothesis that a slight rotation takes place, DFT calculations were performed only on that portion of the MOF. Figure 7 confirms that there is a strong dependence of the C−C inter-ring vibrational frequency on the angle between the planes of benzene rings of the bpdc ligand from a starting position of ∼30°. A 1−2° increase in the angle is sufficient to induce a ∼−15 cm^{-1} red-shift in the C−C inter-ring vibrational frequency, which is consistent with the experimental observation.

Two other experimental observations consistent with a twist of the bpdc ligand: First is the ∼+10 cm^{-1} blue-shift of the ν(C−O) mode, associated with a shortening of the C−O bond at the Zn−O−C node, expected to occur as a result of an increase in angle between one benzene ring relative to the other. Second is the drastic decrease in intensity of the C═O mode

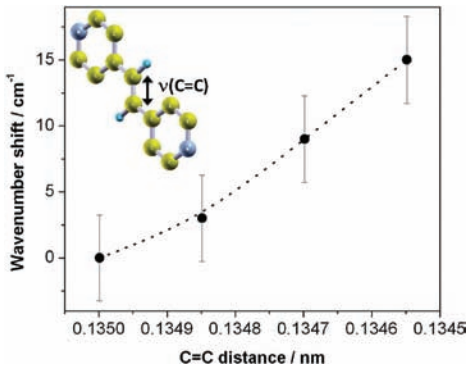

Figure 9. Calculated frequency shifts of C═C in the bpee ligand as a function of bond length. A blue-shift is observed with compression of the bond.

shown in Figure 2, likely due to a twist of the bpdc at the top and the bottom of the bpee ligand (causing such a twist within the two parallel 2D nets to align the uncoordinated C═O entities to point in opposite directions). In this configuration, the opposite electrostatic forces will reduce the atomic displacement of these atoms and cause a decrease in Raman intensity. To confirm this hypothesis, we performed DFT calculations to estimate the change in Raman intensity of the C═O as a function of the angle between the two closest C═O entities of two parallel 2D $Zn_2(bpdc)_2$ layers, as summarized in Figure 8. The intensity of the Raman band of the C═O, calculated according to a model reported by Yamaguchi et al.,[54] decreases as the two C═O align in opposite directions, in support of the proposed mechanism.

Interaction of CO_2 with the bpee Ligand. Information about the overall structure of the MOF can also be indirectly deduced from the changes in the Raman spectra. For instance, the blue-shift of the ν(C═C) mode in the bpee ligand may be attributed to two factors. First, it may be a result of the interaction of CO_2 through its oxygen with the ethylene of the bpee ligand. Indeed, the vdW-DFT2 calculations show that the CO_2 is located ∼3.5 Å from the C═C bond of the bpee and interacts with it through its oxygen. Second, the blue-shift may also indicate a shortening of the C═C as a result of the twist in the bpdc ligand (see Supporting Information Figure S1 for more details). Indeed, the dependence of the Raman frequency shift on the length change of the C═C was determined by DFT calculations. Figure 9 shows the calculated frequency shifts as a function of the C═C length. A blue-shift of ∼2.5 cm^{-1} in the C═C vibrational frequency, observed in the Raman spectra upon CO_2 loading, is calculated to correspond to a $\sim 5 \times 10^{-3}$ nm shortening of the C═C bond. The twist of the bpdc ligand and the C═C bond shortening suggest that the bpee ligand tilts, reducing the *a*-axis length. This tilt modifies the initially distorted parallelogram with a long *a*-axis by making the structure more rectangular with a more open pore, thereby allowing CO_2 to adsorb into the pores. The flexibility of the bpee linker, facilitating changes in tilt angle of the bpee linker in response to CO_2 adsorption, has previously been noted by Culp et al.[10]

4.2. Preferential Adsorption of CO_2 over N_2 at Room Temperature. To understand the role of CO_2 in inducing pore opening, it is important to determine how CO_2 interacts with the structure by examining the data obtained at pressures below the pore-opening pressure ($P < 0.1$ atm) and to compare with data obtained in well-studied nonflexible MOFs. For instance, the

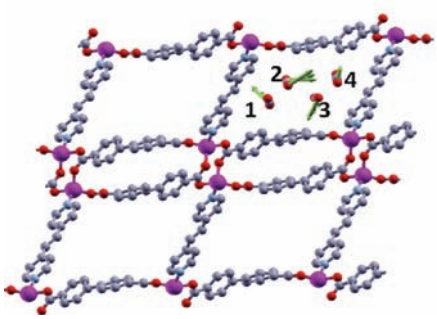

Figure 10. Adsorption sites of CO_2 in complete occupation in $Zn_2(bpdc)_2(bpee)$ determined by vdW-DFT2, where each pore within a unit cell is occupied by four CO_2 molecules. Other pores are similarly occupied by symmetry. Sites 1 and 4 are the lower energy adsorption positions, while sites 2 and 3 are the higher energy ones. The arrows indicate the change in position as the unit cell is loaded and are 5 times amplified.

shifts observed for the asymmetric stretch of CO_2 adsorbed in $Zn_2(bpdc)_2(bpee)$ at pressures 2−6 Torr, ∼−15 cm^{-1}, are larger than the shifts observed for CO_2 adsorbed in MOF-74-Mg, ∼−2 cm^{-1} (see Figure S6 in the Supporting Information), for measurements performed at pressures below 0.1 atm. Neutron diffraction studies performed on MOF-74-Mg have shown that the adsorption of CO_2 is mediated by the oxygen.[55] The larger red-shifts (∼−15 cm^{-1}) observed for $Zn_2(bpdc)_2(bpee)$ suggest that the interaction of CO_2 with the framework at these conditions involves the carbon instead of the oxygen atom. This would indicate that the carbon of the CO_2 is interacting with the C−C bond of the bpdc, causing the most perturbation to the CO_2 asymmetric stretch. Indeed, vdW-DFT2 calculations at a loading of 1 CO_2 molecule/unit cell show that the carbon atom of the CO_2 molecule is located ∼3.6 Å from the C−C inter-ring of the bpdc, compared to ∼3.8 Å between the oxygen in the CO_2 and the same C−C bond (an illustration of CO_2 adsorbed at site 1 is shown in Figure S10 in the Supporting Information). Moreover, twisting of the bpdc ligand, experimentally deduced and supported by DFT calculations, can be caused by weakening of the C−C inter-ring bond (becoming slightly electron deficient) due to the interaction with CO_2. Since this twist occurs only when the CO_2 is introduced (i.e., not with N_2, as summarized in Figure S3 in the Supporting Information), we suggest that it may be due to the larger quadrupole moment of CO_2 (∼4.3 × 10^{26}/esu cm^2) as compared to that of N_2 (∼1.52 × 10^{26}/esu cm^2). This small structural change facilitates the uptake of CO_2 into the pores, which is favorable because its binding energy is even larger after pore opening (33 kJ/mol compared to 29 kJ/mol prior to pore opening).[37]

Higher Loading of CO_2 in $Zn_2(bpdc)_2(bpee)$. At temperatures below ∼−60 °C, the rotational modes of the CO_2 molecules freeze, increasing the residence time of CO_2 molecules in the energetically favorable configuration. This phenomenon results in a sharper CO_2 band, as shown in Figure 4, than at room temperature where the measured frequency is an average of all the relative orientations of the CO_2. Changes in the bands related to the MOF are also observed as the temperature is lowered. These changes include a red-shift of the band at 1646 cm^{-1}, assigned to the C═C stretching mode of the bpee ligand, a decrease in intensity of the inter-ring C−C stretching mode of the bpdc ligand at 1282 cm^{-1}, and a decrease in intensity of the C−O stretching mode at 1363 cm^{-1}. The weakening of the C−C band intensity might be merely a temperature effect, similar to changes observed as a function of temperature in a vacuum (section 3.2, Figure 3). The red-shift of the C═C band suggests a change in the interaction of CO_2 with the bpee ligand. The origin of this change as more CO_2 is loaded and new sites are occupied is likely the CO_2−CO_2 interactions pushing the original CO_2 to a new position, where it has a slightly weaker interaction with the C═C bond of the bpee ligand. VdW-DFT2 calculations performed as more CO_2 is loaded into the framework clearly show a displacement of the CO_2 molecules from their original positions at low loading (Figure 10). For clarity, the arrows in Figure 10 are 5 times larger than their actual values. The CO_2 at the new position is still interacting through its carbon with the C−C inter-ring of the bpdc, but now its distance to that C−C bond is reduced to ∼3.4 Å (from 3.6 Å when there is only 1 CO_2/unit cell).

The energy map derived from vdW-DFT2 calculations, determined to be ∼16 CO_2 molecules/unit cell as shown in Figure 10, makes it possible to compare all the site energies at saturation. The sites labeled 1 and 4, closer to the C−C bond of the bpdc and C═C bond of the bpee ligands, are the most energetically favorable sites. The energies for sites 2 and 3, which are on top of the benzene and pyridine rings, are calculated to be ∼10 kJ/mol higher than those for sites 1 and 4. This finding is somewhat unexpected because the site at the top of the benzene ring is often thought to be the most probable for CO_2 because of the presence of π electrons.

Finally, the Raman and IR frequency shifts of the symmetric and asymmetric stretches (shift from unperturbed frequencies) calculated for adsorbed CO_2 at low loading (site 1) are ∼−3 and −8 cm^{-1}, respectively, and do not vary appreciably as the loading is increased (calculated shifts are −2 and −7 cm^{-1}, respectively). Comparatively, the response of the MOF vibrational modes is larger upon CO_2 loading (e.g., C═C mode shifts by +4 cm^{-1}, C−C inter-ring shifts by −3 cm^{-1}). The interaction of the CO_2 itself is not substantially changed. Shifts in the MOF bands observed for $Zn_2(bpdc)_2(bpee)$ as a function of temperature in the presence of CO_2 are not observed for a rigid framework such as MOF-74-Ni under similar conditions (see Figure S9 in the Supporting Information). They therefore reflect the framework's flexibility and are important measures of the guest−host interaction not always evident in the vibrational modes of the guest.

4.3. Adsorption of N_2 at Low Temperatures. At low temperatures, N_2 can also be incorporated into $Zn_2(bpdc)_2(bpee)$. Isotherms of N_2 performed at −196 °C show a pressure dependence similar to the stepped curve observed for CO_2 at room temperature.[37] Raman spectra collected after introduction of 1 atm of N_2 at −190 °C (Figure 6) also show that the MOF structure undergoes structural changes similar to those observed after CO_2 adsorption at room temperature. However, the adsorption mechanism appears different in this case because N_2 does not adsorb as strongly as CO_2 at room temperature. Consequently, lower temperatures are necessary to physically adsorb on a surface and to balance the molecule's kinetic/rotational energy and the weak attractive energy within the MOF structure. Once these energies are rebalanced, the same phenomenon of pore opening can take place. The longer residence time at a specific configuration allows the interaction with the framework in a way that induces a pore opening, thus allowing the N_2 to enter to the pore.

If the temperature is lowered in the presence of N_2 at atmospheric pressure instead of introducing N_2 at low temperature, the results shown in Figure 5 indicate that there are unexpected changes in the Raman bands occurring at intermediate temperatures (the shift of the C═C bond is not monotonic upon cooling, changing directions at −100 and −180 °C). Indeed, the bands related to the C−O and the C═O stretch modes begin to shift at −100 °C, which indicates that the adsorption starts at this temperature. When N_2 is aligned in a certain configuration with respect to the C−C inter-ring bond, a twist in the bpdc ligand may occur, which would also cause the blue-shift in the C−O stretching at 1355 cm^{-1}. As the temperature nears the triple point of N_2 (−190 °C, 1 atm), additional changes occur. At this point the rotational bands of N_2 freeze and the N_2 can be aligned and remain in the configuration that is the most energetically favorable. The shift back in frequency of the band at 1365 cm^{-1} might be a result of a change in the structure (relaxation) as the temperature is decreased. Similarly, the intensity of the C−C stretch mode is decreased due to a temperature effect similar to that observed in a vacuum as a function of temperature (section 3.2, Figure 3). These findings underscore the differences between N_2 and CO_2, requiring lower temperatures for N_2 to induce adsorption dominated by kinetics effects rather than interactions.

5. CONCLUSIONS

In this work, the interactions of CO_2 and N_2 in a flexible MOF system, $Zn_2(bpdc)_2(bpee)$, were examined, combining Raman and IR spectroscopy with density functional calculations. The connectivity of the ligand to the framework was shown to be a key to the framework's flexibility and to the pore-opening phenomenon. In particular, the monodentate connectivity of the carboxylate of the bpdc ligand to the metal center is the main factor allowing the bpdc ligand to twist, thus providing a path for opening the pore. The changes occurring in the bpee Raman bands were used as the best indicators for this ligand's flexibility.

The preferential adsorption of CO_2 over N_2 is believed to arise from the comparatively larger quadrupole moment of CO_2. The IR data suggest that the interaction of the CO_2 with the bpdc ligand through its carbon weakens the C−C inter-ring of the bpdc ligand, allowing it to rotate slightly around the C−O−Zn node. This rotation causes a series of changes resulting in pore opening. The spectral changes associated with the bpee ligand indicate a C═C bond shortening and/or an interaction with CO_2 through its oxygen. Using the Raman data at lower temperatures and vdW-DFT2 calculations, the total number of adsorption sites (16 CO_2/unit cell) has been identified, and the energetically favorable positions have been shown to be closer to the C═C bond of the bpee and the C−C inter-ring of the bpdc than to the benzene and pyridine rings. The interaction of CO_2 with the C═C bond of the bpee ligand is facilitated through its oxygen, while the interaction with the C−C inter-ring of the bpdc ligand is mediated by the carbon of the CO_2 molecule. At higher loadings, the initial positions of the CO_2 molecules change due to CO_2−CO_2 interactions, causing a slight weakening of the CO_2 interaction with the bpee ligand, consistent with the experimental observations.

■ ASSOCIATED CONTENT

Ⓢ Supporting Information. Crystal structures of $Zn_2(bpdc)_2(bpee)$; treatment of CO_2 IR data; similarity of the Raman spectra of $Zn_2(bpdc)_2(bpee)$ in a vacuum and after N_2 adsorption at room temperature; high-pressure IR measurement of N_2 adsorbed in $Zn_2(bpdc)_2(bpee)$ at room temperature; isotherms of CO_2 adsorption at different temperatures as a function of pressure; IR frequency of CO_2 adsorbed onto MOF-74-Mg; characterization of $Zn_2(bpdc)_2(bpee)$; Raman spectra of MOF-74-Ni as a function of temperature in the presence of CO_2; illustration of CO_2 adsorbed at site 1; and complete author list of references 43 and 45. This material is available free of charge via the Internet at http://pubs.acs.org.

■ AUTHOR INFORMATION

Corresponding Author
chabal@utdallas.edu

■ ACKNOWLEDGMENT

This work is supported fully by the U.S. Department of Energy (DOE Grant No. DE-FG02-08ER46491). P.T. gratefully acknowledges the DFG for their financial support.

■ REFERENCES

(1) Uemura, T.; Yanai, N.; Kitagawa, S. *Chem. Soc. Rev.* **2009**, *38*, 1228–1236.
(2) Murray, L. J.; Dinca, M.; Long, J. R. *Chem. Soc. Rev.* **2009**, *38*, 1294–1314.
(3) Lee, J.; Farha, O. K.; Roberts, J.; Scheidt, K. A.; Nguyen, S. T.; Hupp, J. T. *Chem. Soc. Rev.* **2009**, *38*, 1450–1459.
(4) Li, J.-R.; Kuppler, R. J.; Zhou, H.-C. *Chem. Soc. Rev.* **2009**, *38*, 1477–1504.
(5) Kuppler, R. J.; Timmons, D. J.; Fang, Q.-R.; Li, J.-R.; Makal, T. A.; Young, M. D.; Yuan, D.; Zhao, D.; Zhuang, W.; Zhou, H.-C. *Coord. Chem. Rev.* **2009**, *253*, 3042–3066.
(6) Tran, U. P. N.; Le, K. K. A.; Phan, N. T. S. *ACS Catal.* **2011**, *1*, 120–127.
(7) Férey, G.; Mellot-Draznieks, C.; Serre, C.; Millange, F.; Dutour, J.; Surble, S.; Margiolaki, I. *Science* **2005**, *309*, 2040–2042.
(8) Férey, G.; Serre, C. *Chem. Soc. Rev.* **2009**, *38*, 1380–1399.
(9) Salles, F.; Maurin, G.; Serre, C.; Llewellyn, P. L.; Knofel, C.; Choi, H. J.; Filinchuk, Y.; Oliviero, L.; Vimont, A.; Long, J. R.; Férey, G. *J. Am. Chem. Soc.* **2010**, *132*, 13782–13788.
(10) Culp, J. T.; Smith, M. R.; Bittner, E.; Bockrath, B. *J. Am. Chem. Soc.* **2008**, *130*, 12427–12434.
(11) Bureekaew, S.; Shimomura, S.; Kitagawa, S. *Sci. Technol. Adv. Mater.* **2008**, *9*, 014108.
(12) Jin, X.-H.; Sun, J.-K.; Cai, L.-X.; Zhang, J. *Chem. Commun.* **2011**, *47*, 2667–2669.
(13) Férey, G. *Chem. Soc. Rev.* **2008**, *37*, 191–214.
(14) Tanaka, D.; Nakagawa, K.; Higuchi, M.; Horike, S.; Kubota, Y.; Kobayashi, T. C.; Takata, M.; Kitagawa, S. *Angew. Chem.* **2008**, *120*, 3978–3982.
(15) Mulfort, K. L.; Farha, O. K.; Malliakas, C. D.; Kanatzidis, M. G.; Hupp, J. T. *Chem. Eur. J.* **2010**, *16*, 276–281.
(16) Kitaura, R.; Seki, K.; Akiyama, G.; Kitagawa, S. *Angew. Chem., Int. Ed.* **2003**, *42*, 428–431.
(17) Demessence, A.; Long, J. R. *Chem. Eur. J.* **2010**, *16*, 5902–5908.
(18) Hamon, L.; Llewellyn, P. L.; Devic, T.; Ghoufi, A.; Clet, G.; Guillerm, V.; Pirngruber, G. D.; Maurin, G.; Serre, C.; Driver, G.; van Beek, W.; Jolimaître, E.; Vimont, A.; Daturi, M.; Férey, G. R. *J. Am. Chem. Soc.* **2009**, *131*, 17490–17499.
(19) Fernandez, C. A.; Thallapally, P. K.; Motkuri, R. K.; Nune, S. K.; Sumrak, J. C.; Tian, J.; Liu, J. *Cryst. Growth Des.* **2010**, *10*, 1037–1039.
(20) Yang, C.; Wang, X.; Omary, M. A. *J. Am. Chem. Soc.* **2007**, *129*, 15454–15455.

(21) Yang, C.; Wang, X.; Omary, M. A. *Angew. Chem., Int. Ed.* **2009**, *48*, 2500–2505.
(22) Coudert, F. X.; Jeffroy, M.; Fuchs, A. H.; Boutin, A.; Mellot-Draznieks, C. *J. Am. Chem. Soc.* **2008**, *130*, 14294–14302.
(23) Yang, C.; Wang, X.; Omary, M. A. *Angew. Chem., Int. Ed.* **2009**, *48*, 2500–2505.
(24) Llewellyn, P. L.; Maurin, G.; Devic, T.; Loera-Serna, S.; Rosenbach, N.; Serre, C.; Bourrelly, S.; Horcajada, P.; Filinchuk, Y.; Férey, G. *J. Am. Chem. Soc.* **2008**, *130*, 12808–12814.
(25) Serre, C.; Bourrelly, S.; Vimont, A.; Ramsahye, N. A.; Maurin, G.; Llewellyn, P. L.; Daturi, M.; Filinchuk, Y.; Leynaud, O.; Barnes, P.; Férey, G. *Adv. Mater.* **2007**, *19*, 2246–2251.
(26) Siberio-Perez, D. Y.; Wong-Foy, A. G.; Yaghi, O. M.; Matzger, A. J. *Chem. Mater.* **2007**, *19*, 3681–3685.
(27) Centrone, A.; Siberio-Pérez, D. Y.; Millward, A. R.; Yaghi, O. M.; Matzger, A. J.; Zerbi, G. *Chem. Phys. Lett.* **2005**, *411*, 516–519.
(28) Vitillo, J. G.; Regli, L.; Chavan, S.; Ricchiardi, G.; Spoto, G.; Dietzel, P. D. C.; Bordiga, S.; Zecchina, A. *J. Am. Chem. Soc.* **2008**, *130*, 8386–8396.
(29) Nijem, N.; Veyan, J.-F.; Kong, L.; Wu, H.; Zhao, Y.; Li, J.; Langreth, D. C.; Chabal, Y. J. *J. Am. Chem. Soc.* **2010**, *132*, 14834–14848.
(30) Nijem, N.; Veyan, J.-F.; Kong, L.; Li, K.; Pramanik, S.; Zhao, Y.; Li, J.; Langreth, D.; Chabal, Y. J. *J. Am. Chem. Soc.* **2010**, *132*, 1654–1664.
(31) Bordiga, S.; Vitillo, J. G.; Ricchiardi, G.; Regli, L.; Cocina, D.; Zecchina, A.; Arstad, B.; Bjorgen, M.; Hafizovic, J.; Lillerud, K. P. *J. Phys. Chem. B* **2005**, *109*, 18237–18242.
(32) Valenzano, L.; Civalleri, B.; Chavan, S.; Palomino, G. T.; Arean, C. O.; Bordiga, S. *J. Phys. Chem. C* **2010**, *114*, 11185–11191.
(33) Allendorf, M. D.; Houk, R. J. T.; Andruszkiewicz, L.; Talin, A. A.; Pikarsky, J.; Choudhury, A.; Gall, K. A.; Hesketh, P. J. *J. Am. Chem. Soc.* **2008**, *130*, 14404–14405.
(34) Nijem, N.; Kong, L.; Zhao, Y.; Wu, H.; Li, J.; Langreth, D. C.; Chabal, Y. J. *J. Am. Chem. Soc.* **2011**, *133*, 4782–4784.
(35) Huang, Y.; Havenga, E. A. *Chem. Mater.* **2001**, *13*, 738–746.
(36) Lan, A. J.; Li, K. H.; Wu, H. H.; Kong, L. Z.; Nijem, N.; Olson, D. H.; Emge, T. J.; Chabal, Y. J.; Langreth, D. C.; Hong, M. C.; Li, J. *Inorg. Chem.* **2009**, *48*, 7165–7173.
(37) Wu, H.; Reali, R. S.; Smith, D. A.; Trachtenberg, M. C.; Li, J. *Chem. Eur. J.* **2010**, *16*, 13951–13954.
(38) Hafner, J. *J. Comput. Chem.* **2008**, *29*, 2044–2078.
(39) Dion, M.; Rydberg, H.; Schroder, E.; Langreth, D. C.; Lundqvist, B. I. *Phys. Rev. Lett.* **2005**, *95*, No. 109902.
(40) Dion, M.; Rydberg, H.; Schröder, E.; Langreth, D. C.; Lundqvist, B. I. *Phys. Rev. Lett.* **2004**, *92*, No. 246401.
(41) Thonhauser, T.; Cooper, V. R.; Li, S.; Puzder, A.; Hyldgaard, P.; Langreth, D. C. *Phys. Rev. B* **2007**, *76*, No. 125112.
(42) Lee, K.; Murray, É. D.; Kong, L.; Lundqvist, B. I.; Langreth, D. C. *Phys. Rev. B* **2010**, *82*, No. 081101.
(43) Gonze, X.; et al. *Comput. Phys. Commun.* 2009, *180*, 2582–2615.
(44) Gonze, X.; et al. *Z. Kristallogr.* **2005**, *220*, 558–562.
(45) Langreth, D. C.; et al. *Comput. Phys. Commun.* **2009**, *180*, 2582–2615.
(46) Kleis, J.; Lundqvist, B. I.; Langreth, D. C.; Schröder, E. *Phys. Rev. B* 2007, *76*, No. 100201.
(47) Cooper, V. R.; Thonhauser, T.; Puzder, A.; Schröder, E.; Langreth, D. C. *J. Am. Chem. Soc.* 2008, *130*, 1304–1308.
(48) Kong, L.; Cooper, V. R.; Nijem, N.; Li, K.; Li, J.; Chabal, Y. J.; Langreth, D. C. *Phys. Rev. B* 2009, *79*, No. 081407.
(49) Kong, L.; Roman-Perez, G.; Soler, J. M.; Langreth, D. C. *Phys. Rev. Lett.* 2009, *103*, No. 096103.
(50) Troullier, N.; Martins, J. L. *Phys. Rev. B* 1991, *43*, 1993.
(51) Perdew, J. P.; Burke, K.; Ernzerhof, M. *Phys. Rev. Lett.* 1996, *77*, 3865–3868.
(52) Hou, X.; Wu, L.; Xu, W.; Qin, L.; Wang, C.; Zhang, X.; Shen, J. *Colloids Surf., A* **2002**, *198−200*, 135–140.
(53) Nakamoto, K. *Infrared and Raman Spectra of Inorganic and coordination compounds*, 5th ed.; John Wiley and Sons Inc.: New York, 1997, Part B.
(54) Yamaguchi, S.; Yoshimizu, N.; Maeda, S. *J. Phys. Chem.* **1978**, *82*, 1078–1080.
(55) Wu, H.; Simmons, J. M.; Srinivas, G.; Zhou, W.; Yildirim, T. *J. Phys. Chem. Lett.* **2010**, *1*, 1946–1951.